ARTICLE

Photostability of 2,6-Diaminopurine and its 2'-Deoxyriboside Investigated by Femtosecond Transient Absorption Spectroscopy

Received 00th January 20xx,
Accepted 00th January 20xx

DOI: 10.1039/x0xx00000x

Naishka E. Caldero-Rodríguez,[a‡] Luis A. Ortiz-Rodríguez,[a‡] Andres A. Gonzalez,[a⊥] Carlos E. Crespo-Hernández*[a]

Ultraviolet radiation (UVR) from the sun is essential for the prebiotic syntheses of nucleotides, but it can also induce photolesions such as the cyclobutane pyrimidine dimers (CPDs) to RNA or DNA oligonucleotide in prebiotic Earth. 2,6-Diaminopurine (26DAP) has been proposed to repair CPDs in high yield under prebiotic conditions and be a key component in enhancing the photostability of higher-order prebiotic DNA structures. However, its electronic relaxation pathways have not been studied, which is necessary to know whether 26DAP could have survived the intense UV fluxes of the prebiotic Earth. We investigate the electronic relaxation mechanism of both 26DAP and its 2'-deoxyribonucleoside (26DAP-d) in aqueous solution using steady-state and femtosecond transient absorption measurements that are complemented with electronic-structure calculations. The results demonstrate that both purine derivatives are significantly photostable to UVR. It is shown that upon excitation at 287 nm, the lowest energy $^1\pi\pi^*$ state is initially populated. The population then branches following two relaxation coordinates in the $^1\pi\pi^*$ potential energy surface, which are identified as the C2- and C6-relaxation coordinates. The population following the C6-coordinate internally converts to the ground state nonradiatively through a nearly barrierless conical intersection within 0.7 ps in 26DAP or within 1.1 ps in 26DAP-d. The population that follows the C2-relaxation coordinate decays back to the ground state by a combination of nonradiative internal conversion via a conical intersection and fluorescence emission from the $^1\pi\pi^*$ minimum in 43 ps and 1.8 ns for the N9 and N7 tautomers of 26DAP, respectively, or in 70 ps for 26DAP-d. Fluorescence quantum yields of 0.037 and 0.008 are determined for 26DAP and 26DAP-d, respectively. Collectively, it is demonstrated that most of the excited state population in 26DAP and 26DAP-d decays back to the ground state via both nonradiative and radiative relaxation pathways. This result lends support to the idea that 26DAP could have accumulated in large enough quantities during the prebiotic era to participate in the formation of prebiotic RNA or DNA oligomers and act as a key component in the protection of the prebiotic genetic alphabet.

Introduction

The cyclobutane pyrimidine dimers (CPDs) are the most frequent UV-induced photolesions occurring at bipyrimidine sites of nucleic acid strands.[1,2] CPDs can block DNA replication and transcription and lead to plant growth inhibition,[3] mutagenesis, activation of protooncogenes, and ultimately carcinogenesis.[4–6] Nature has developed strategies, such as photolyase-mediated repair and nucleotide excision (NER) repair mechanisms, to mend these photolesions.[7–10] However, photolyases and the more complex NER appeared in evolution after the first organisms emerged and could not have contributed to photodamage repair of the initial prebiotic oligonucleotides. Thus, it is postulated that more primitive mechanisms should have protected their integrity during the prebiotic era.[11,12] Recently, Szabla et al. demonstrated that by replacing the canonical nucleobase adenine with a purine derivative, 2,6-diaminopurine (26DAP), CPDs can be repaired in yields reaching 92% under prebiotic conditions due to the excellent electron-donating properties of 26DAP in nucleic acid strands.[13] They further proposed that 26DAP could have been formed on prebiotic Earth alongside adenine through a transglycosylation reaction.[13] Interestingly, scientists from the National Aeronautics and Space Administration (NASA) showed that carbon-rich meteorites could have also provided the prebiotic Earth with 26DAP because it was identified in the meteorites Murchison and LON 94102 together with purine and 6,8-diaminopurine.[14] 26DAP can base pair with thymine in a non-Watson-Crick manner creating a stronger base pair than that between thymine and adenine because the amino group at position C2 makes available a third hydrogen bonding site.[15–17] Furthermore, it has been shown that 26DAP replaces adenine in the genome of phage S-2L of the cyanobacteria *Synechococcus elongatus* entirely,[15–17] and can increase the rate of nonenzymatic RNA template copying.[18] The deoxyriboside (26DAP-d) can also undergo prebiotic phosphorylation and concomitant oligomerization to form DNA,[19] which could have been key in the development of higher-order oligomeric structures. Therefore, 26DAP may be considered an important component in protecting the prebiotic genetic material, thus enhancing the photostability of higher-order DNA structures and the formation of the first DNA oligomers.

For 26DAP to have played an important role in the prebiotic era, it would have needed to survive long enough to accumulate in significant quantities during the prebiotic Earth conditions. In particular, protection against strong UV radiation was likely a

[a]*Department of Chemistry, Case Western Reserve University, Cleveland, OH 44106.*
**Corresponding author; E-mail: carlos.crespo@case.edu; ORCID: 000-0002-3594-0890.*
‡ contributed equally to this work; ⊥ participated as an undergraduate research assistant.
†Electronic Supplementary Information (ESI) available: Excitation spectra, relevant optimized geometries of 26DAP and 26DAP-d and excited state absorption spectra of key points in the potential energy surface of 26DAP.
See DOI: 10.1039/x0xx00000x

Please do not adjust margins

decisive selection criterion,[20] and thus, the photostability of prebiotic components must be studied when proposing their potential availability and participation in prebiotic chemistry.[21] To the best of our knowledge, however, the excited state relaxation pathways and photostability of 26DAP following UV excitation have not been investigated.

In this contribution, steady-state absorption and emission spectroscopies and femtosecond broadband transient absorption spectroscopy are complemented with electronic-structure calculations to investigate the photochemistry of 26DAP and 26DAP-d in aqueous solutions to delineate their electronic deactivation mechanisms and to shed some light on their possible availability during the prebiotic Earth.

Experimental and theoretical methods

Chemicals

2,6-diaminopurine (26DAP) was purchased from Sigma-Aldrich, Inc. (98% purity), and 2,6-diaminopurine-2'-deoxyribose (26DAP-d) was obtained from Chem-Impex International, Inc. (99.9% purity). 26DAP and 26DAP-d were used as received. The phosphate buffer at pH 7.4 was freshly prepared using monopotassium and dipotassium phosphate salts in ultrapure water with a total phosphate concentration of 16 mM. The pH of the solution was adjusted using a solution of sodium hydroxide (0.1 M).

Steady-state measurements

The steady-state absorption measurements were obtained using a Cary 300 Bio spectrophotometer. The steady-state emission measurements were obtained using a Cary Eclipse spectrofluorometer. The parameters used to obtain the emission spectra include a scan rate of 120 nm min^{-1}, 5 nm slit widths, and a PMT voltage of 600 V. Fluorescence quantum yield measurements were performed using tryptophan as the standard.[22] To minimize inner filter effects, these measurements were obtained utilizing samples with an optical density of <0.2 at the excitation wavelength.

Electronic-structure calculations

All electronic-structure calculations were performed in ORCA 5.0.[23] To determine the ground state composition of 26DAP and 26DAP-d, optimizations were performed with the B3LYP hybrid functional[24] and the cc-pVDZ basis set.[25] The conductor-like polarizable continuum model (CPCM)[26] was used to implicitly model bulk solvation. To increase the efficiency of the calculations, the RIJCOSX density fitting approximation was employed.[27] This density fitting approximation decomposed the usual four-centered two-electron integrals into three-centered integrals using the corresponding auxiliary basis set. In the case of 26DAP, to refine the relative energy among tautomers, three explicit water molecules were added to form hydrogen bonds with the nitrogens of the purine core of the two most stable tautomers and were reoptimized. The percentage of ground state composition (P) at room temperature of the tautomers were calculated using equations (1) and (2):[22]

$$P = e^{-\Delta E/kT}/Z \quad (1)$$

$$Z = \sum e^{-\Delta E/kT} \quad (2)$$

where, $e^{-\Delta E/kT}$ is the ratio of the population of a particular species, Z is the sum of the possible species, k is the Boltzmann's constant (units: eV K^{-1}), and T is the temperature (298 K).

Vertical excitation energies from ground state optimized geometries were calculated at the TD-BP86[28]/CPCM/def2-TZVP[29]//B3LYP/cc-pVDZ level of theory in water. The character of the first excited singlet state was determined based on the magnitude of the oscillator strength and by visual inspection of the Kohn-Sham orbitals. All excited state and conical intersection optimizations were performed at the TD-B3LYP/cc-pVDZ level of theory using the RIJCOSX density fitting approximation. Potential energy profiles were generated at the TD-BP86/CPCM/def2-TZVP level of theory in water.

Femtosecond broadband transient absorption spectroscopy

The transient absorption setup used in this study has been described in detail elsewhere.[30] The TAS spectrometer (Helios, Ultrafast Systems) uses a Ti:Sapphire oscillator (Vitesse, Coherent) that seeds a regenerative amplifier (Libra-HE, Coherent), generating pulses of 100 fs (1 kHz and 800 nm). The generation of the 287 nm beam was done by pumping an optical parametric amplifier (TOPAS, Quantronix/Light conversion). The excitation pulses were set to a power of 0.75 or 0.5 mW for 26DAP and 26DAP-d, respectively, measured at the optical cell position. A translating 2 mm CaF_2 crystal generates the white light continuum, which gives access to a spectral range from 320 to 700 nm. Fused silica cells with a 2 mm path length were used for the transient absorption measurements. To ensure the irradiation of fresh volume of the solution, a Teflon-coated magnetic bar was used to continuously stir the solutions throughout the experiments. Freshly prepared samples were used in each experiment. The data collection and pre-processing were performed in a homemade LabView-based software, while the global and target analyses of the transient data analysis were done using the Glotaran graphical user interface to the R-package TIMP software.[31]

Results

Steady-state photophysics

26DAP and 26DAP-d consist of a purine core chromophore containing two amino groups in the C2 and C6 positions, with 26DAP-d also being glycosylated at the N9 position with 2'-deoxyribose (Scheme 1). Two pK_a values have been reported for 26DAP in water: a pK_1 of 5.09 and a pK_2 of 10.77.[32] Moreover, a pK_a of 5.4 has been reported for the 2,6-diaminopurine riboside (26DAP-r). Herein, we assume a similar pK_a value for 26DAP-d compared to 26DAP-r.

 This journal is © The Royal Society of Chemistry 20xx

Please do not adjust margins

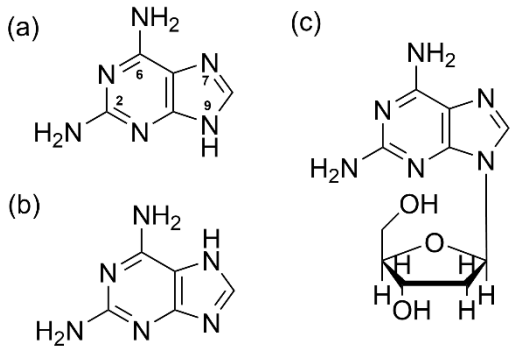

Scheme 1. Structures of the (a) N9 and (b) N7 tautomers of 2,6-diaminopurine (26DAP), and (c) 2,6-diaminopurine-2'-deoxyribose (26DAP-d). Standard ring numbering has been included.

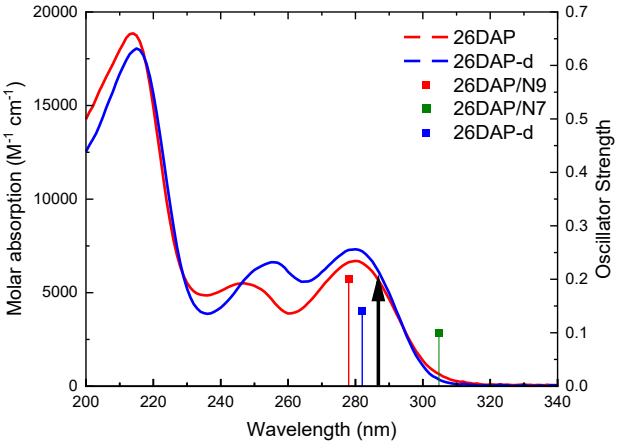

Figure 1. Molar absorption spectra of 26DAP (solid red line) and 26DAP-d (solid blue line) in phosphate buffer pH 7.4, together with the calculated lowest-energy electronic transition and corresponding oscillator strengths for the N9 (vertical red line) and N7 (vertical green line) tautomers of 26DAP and 26DAP-d (vertical blue line) in water at the TD-BP86/CPCM/def2-TZVP//B3LYP/cc-pVDZ level of theory. The black arrow indicates the excitation wavelength used for the transient absorption measurements at 287 nm.

Using these pK_a values and the Henderson-Hasselbalch relationship, it was determined that 26DAP and 26DAP-d are present as neutral species (>99%) at physiological conditions of pH 7.4. Therefore, from this point forward, we consider exclusively the neutral forms of both 26DAP and 26DAP-d.

Figure 1 presents the molar absorption spectra of 26DAP and 26DAP-d in phosphate buffer pH 7.4. The molar absorption spectrum of 26DAP contains three bands with maxima at 280, 247, and 214 nm with values of $(6.7 \pm 0.5) \times 10^3$ M^{-1} cm^{-1}, $(5.6 \pm 0.5) \times 10^3$ M^{-1} cm^{-1}, and $(18.9 \pm 0.7) \times 10^3$ M^{-1} cm^{-1}, respectively, while the molar absorption spectrum of the 26DAP-d contains three bands with maxima at 280, 255, and 215 nm with values of $(6.7 \pm 0.5) \times 10^3$ M^{-1} cm^{-1}, $(6.7 \pm 0.5) \times 10^3$ M^{-1} cm^{-1}, and $(18.1 \pm 0.7) \times 10^3$ M^{-1} cm^{-1}, respectively. It is worth noticing that the absorption tail in 26DAP extends over to 320 nm, while the one observed for 26DAP does not exhibit detectable absorption above 310 nm.

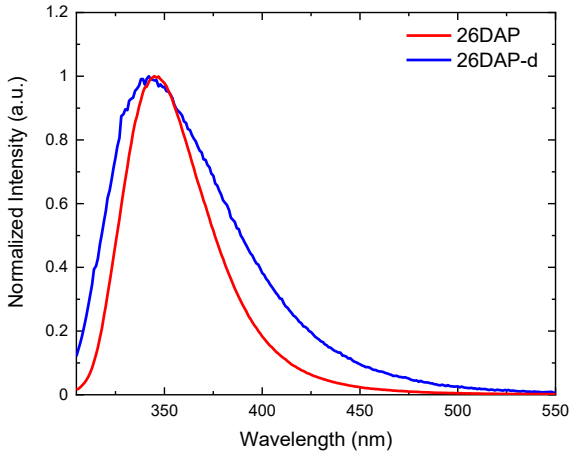

Figure 2. Normalized emission spectra (λ_{exc} = 290 nm) of 26DAP (red) and 26DAP-d (blue) in phosphate buffer pH 7.4.

Figure 2 shows the emission spectra of 26DAP and 26DAP-d in phosphate buffer pH 7.4. The emission spectrum of 26DAP has a maximum at 345 nm, while in 26DAP-d, it has a maximum at 342 nm. Considering the relatively small Stokes' shift observed, the emission is assigned to fluorescence. Fluorescence quantum yields (λ_{exc} = 290 nm) of (0.037 ± 0.003) and (0.008 ± 0.001) were measured for 26DAP and 26DAP-d, respectively. The obtained values are comparable to previously reported values for 26DAP and 26DAP-r of 0.02 and 0.010, respectively.[33,34] The excitation spectra (λ_{em} = 351 nm) of 26DAP and 26DAP-d in phosphate buffer pH 7.4 are reported in Figure S1. The lowest energy band in the excitation spectrum of 26DAP contains a maximum intensity at ca. 291 nm, while 26DAP-d has a maximum intensity at ca. 278 nm. The excitation spectrum of 26DAP is significantly different from that of 26DAP-d. While the excitation spectrum of 26DAP-d agrees with the absorption spectrum, the excitation spectrum of 26DAP is significantly redshifted relative to the absorption spectrum. To discard the possibility of impurity in the sample, 26DAP was recrystallized in water, as previously reported for the recrystallization of adenine,[35] and an identical excitation spectrum was obtained, which suggests that the difference in the excitation spectrum of 26DAP relative to the absorption spectrum is not due to an impurity (Figure S1). Furthermore, the excitation spectrum obtained for 26DAP is in good agreement with that reported by Santhosh et al.[36] Considering that 26DAP at pH 7.4 is in its neutral form, prototropic tautomerization is possible. Therefore, we proposed that the difference between the excitation and the absorption spectrum of 26DAP is due to the contribution of a fluorescent tautomer that exists in solution in smaller amounts than the primary tautomer that contributes to the absorption spectrum. Based on our experimental results, the tautomer that dominates the excitation spectrum should have a significantly higher fluorescence quantum yield than the tautomer that dominates the absorption spectrum. Quantum-chemical calculations presented in the next section support the idea that more than one tautomer of 26DAP is present in solution. Glycosylation in 26DAP-d blocks tautomerization; thus, 26DAP-d is present as a single tautomer in solution, as observed in other purine derivatives.[37–39]

Please do not adjust margins

Ground state composition of 26DAP and 26DAP-d

26DAP exists in its neutral form at pH 7.4. Therefore, only eight neutral tautomers were optimized at the B3LYP/CPCM/cc-pVDZ level of theory in water (Figure S2). Based on the relative energies among tautomers, the N9 (0.00 kcal/mol) and N7 (2.86 kcal/mol) tautomers are the most stable tautomers in water. However, the N7 tautomer has an energy of 2.86 kcal/mol relative to the N9 tautomer, which is above *kT* at room temperature. To examine the role of explicit water molecules in the stabilization energy of these tautomers, three explicit water molecules were added to form hydrogen bonds with the nitrogens of the purine core, and the structures were optimized at the same level of theory (Figure S3). The relative energies at the B3LYP/CPCM/cc-pVDZ level of theory in water among the N9 and N7 tautomers calculated from these geometries are 0.00 and 0.22 kcal/mol, respectively (Figure S3). Evidently, hydrogen bonding stabilizes the N7 tautomer, and considering that its relative energy is below *kT* at room temperature, it is expected to be available in solution in equilibrium with the N9 tautomer. Based on the relative energies, the calculated percentage of ground state composition at room temperature of the N9 and N7 tautomers are ca. 60% and 40%, respectively. The presence of two tautomers in solution of 26DAP is supported by the differences observed between the excitation and the absorption spectrum of 26DAP. Therefore, from this point forward, we focus our investigations on both the N9 and N7 tautomers of 26DAP.

In the case of neutral 26DAP-d, the *syn*- and *anti*-sugar conformations were optimized at the B3LYP/CPCM/cc-pVDZ level of theory in water (Figure S4). The *syn*-sugar conformation is 4.83 kcal/mol more stable than the *anti*- and, thus, is predicted to be the only conformation available in solution at room temperature. Hereafter, all calculations focus on the *syn*-conformation of 26DAP-d.

Vertical excitation energies, excited state optimizations, and potential energy profiles of 26DAP and 26DAP-d

As reported in the previous section, 26DAP is predicted to be available in solution as a mixture of the N9 and N7 tautomers, while 26DAP-d is predicted to be available in its *syn*-conformation. Therefore, our TD-DFT calculations are focused on those structures. To characterize the excited states available for deactivation following UV excitation at the lowest-energy absorption band of 26DAP and 26DAP-d, vertical excitation energies were calculated at the TD-BP86/CPCM/def2-TZVP//B3LYP/cc-pVDZ level of theory in water and are reported in Table 1.

Table 1. Vertical excitation energies (in eV) of 26DAP and 26DAP-d at the TD-BP86/CPCM/def2-TZVP//B3LYP/cc-pVDZ in water.

State*	26DAP/N9	26DAP/N7	26DAP-d
$^1\pi\pi^*$	4.46 (0.20)	4.05 (0.11)	4.39 (0.14)
$^3\pi\pi^*$	3.41	3.15	3.35
$^3\pi\pi^*$	4.20	4.11	4.04

*The S_2 ($n\pi^*$) state for all three molecules has a negligible oscillator strength (f = 0.00) and is high in energy to be directly excited at 287 nm.

The BP86 functional was chosen for the vertical excitation energies calculations over hybrid functionals such as B3LYP, PBE0, and ωB97X because these functionals significantly overestimated the energy of the lowest-energy excited singlet state, as shown in Table S1. Following excitation at the lowest-energy absorption band, the first excited singlet state is predicted to be populated in 26DAP, in both tautomers, and also in 26DAP-d. This state has $\pi\pi^*$ character in both tautomers of 26DAP and in 26DAP-d (Figure S5, S6, and S7) in agreement with the work by Mburu and Matsika at the CASSCF/MRMP2 level.[40] The second lowest singlet state has $n\pi^*$ character (f = 0.00) and is predicted to be high in energy (4.81 eV for 26DAP/N9, 4.47 eV for 26DAP/N7, and 4.51 eV for 26DAP-d) to be accessed directly upon excitation at 287 nm. The vertical excitation energies agree with the experimental observation that the lowest-energy transition in the N7 tautomer is expected to be redshifted relative to that of the N9 tautomer (Figure 1). Furthermore, the oscillator strength of the first excited singlet state in the N7 tautomer is approximately half of that of the N9 tautomer, which may explain why the absorption band of the N7 tautomer cannot be easily resolved in the ground state absorption spectra (i.e., not only the N7 tautomer is expected to be in solution in a smaller amount, but the oscillator strength is predicted to be smaller than that of the N9 tautomer in the lowest-energy $^1\pi\pi^*$ state). There are two triplet states lower in energy than the $^1\pi\pi^*$ state in both tautomers of 26DAP and in 26DAP-d. However, these triplet states have $\pi\pi^*$ character and intersystem crossing to these states from the $^1\pi\pi^*$ is not expected to be favorable and/or efficient based on El-Sayed's propensity rules.[41,42] Indeed, no triplet population is observed in our transient absorption results. This will be discussed in detail in the following sections.

In order to map the potential energy surface of the $^1\pi\pi^*$ state in the N9 and N7 tautomers, optimizations were performed in vacuum at the B3LYP/cc-pVDZ level of theory. Following optimization of the $^1\pi\pi^*$ state (Figure S8), two plausible $^1\pi\pi^*/S_0$ conical intersections were identified for each tautomer (Figure 3 and Figure S8). One conical intersection exhibits significant C6-puckering (CI_{C6}), while the other one exhibits significant C2-puckering (CI_{C2}). Hence, optimizations along the C6-puckering (N6C6C5C4 dihedral angle) and C2-puckering (N2C2N3C4 dihedral angle) coordinates were performed to investigate the accessibility to the putative conical intersections. We are aware of the limitations of linear response (LR) TD-DFT in predicting the correct dimensionality of conical intersections between the ground and excited states. However, in this study, the focus is not on describing the shape of the conical intersections but on getting a reasonable idea of the geometries and

 This journal is © The Royal Society of Chemistry 20xx

Please do not adjust margins

Please do not adjust margins

the energetics in those regions of phase-space. Previous work reported by Martínez and co-workers showed that LR-TD-DFT can predict the geometries and energetics to a reasonable accuracy,[43] and thus, we expect that the methodology employed herein should at least provide a qualitatively correct description of the system. We also note that the conical intersections found in this study are in agreement with those found by Szabla et al.[13] In spite of the known limitations of LR-TD-DFT, we hope that these calculations will motivate more investigations that employ multireference methodologies in the near future.

Figure 3 shows the potential energy profiles constructed along both coordinates for the N9 and N7 tautomers at the TD-BP86/CPCM/def2-TZVP//TD-B3LYP/cc-pVDZ level of theory in water. In both tautomers, CI_{C6} can be accessed nearly barrierless, while a barrier must be overcome to access CI_{C2}. In the N9 tautomer, the energy barrier to access the CI_{C2} amounts 0.4 eV, while in the N7 tautomer, the energy barrier amounts 0.8 eV. Therefore, the excited state population in the C2-puckering coordinate is expected to decay back to the ground state significantly slower than the population in the C6-puckering coordinate.

Moreover, the decay back to the ground state in the N7 tautomer is expected to be slower than in the N9 tautomer due to the larger energy barrier that must be overcome to access CI_{C2}. Finally, the excited state absorption spectra (Figure S9) of the $^1\pi\pi^*$ minimum and CI_{C6} and CI_{C2} for the N9 and N7 tautomers of 26DAP were calculated to aid with the assignment of the transient absorption bands reported in the following section.

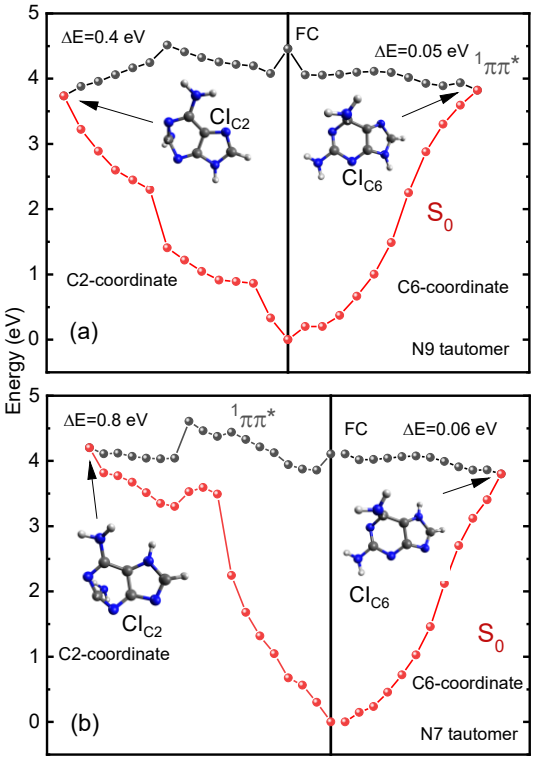

Figure 3. Potential energy profiles of (a) N9 and (b) N7 tautomers along with the C2-puckering and C6-puckering coordinates at the TD-BP86/CPCM/def2-TZVP//TD-B3LYP/cc-pVDZ in water. Inset: Molecular structure of the relevant conical intersections found in the C2-puckering and C6-puckering coordinates for both tautomers. ΔE represents the energy barrier to access the conical intersections.

Femtosecond broadband transient absorption spectroscopy

Femtosecond transient absorption experiments were performed to investigate the electronic relaxation pathways of 26DAP and 26DAP-d. Figure 4 presents the transient absorption spectra of 26DAP and 26DAP-d in phosphate buffer pH 7.4 following excitation at 287 nm. Excitation at 287 nm results in the formation of three transient absorption bands centered at 640, 465, and 390 nm for 26DAP (Figure 4a) and 645, 470, and 395 nm for 26DAP-d (Figure 4d), within the cross correlation of the pump and probe beams. Stimulated emission is observed around 345 nm at time zero in both molecules. After time zero, the amplitude of the transient absorption bands of 26DAP at 465 and 390 nm decreases, and slightly blueshifts to ca. 460 and 385 nm, respectively. This coincides with an increase in intensity of the band with a maximum at ca. 640 nm and simultaneous blueshift to 630 nm (Figure 4b) that forms an apparent isosbestic point at ca. 525 nm. Similarly, a decrease in the amplitude and a simultaneous blueshift of 5 nm is observed in the two transient absorption bands of 26DAP-d below 500 nm, with an increase in intensity of the band above 500 nm that blueshifts by ca. 10 nm, creating an apparent isosbestic point around 525 nm (Figure 4e). Hereafter, the transient bands decay, with the transient species in 26DAP taking significantly longer (ca. hundreds of picoseconds) to decay than the transient species in 26DAP-d (Figure 4c and f, respectively). No evidence of long-lived transient species that could be assigned to $^1n\pi^*$ or triplet states is observed, and the transient absorption spectra for both systems decay within 3 ns. Representative decay traces, lifetimes, and evolution-associated difference spectra (EADS) obtained from the global and target analyses of the transient absorption data are reported in Figure 5, Table 2, and Figure S10, respectively. We note that both 26DAP and 26DAP-d are significantly photostable. We estimate a photodegradation of only 2% and 8%, respectively, from the decrease in absorbance at the absorption maximum of the lowest energy absorption band following irradiation doses of 277 and 246 J cm^{-2} at 287 nm. This supports the idea that photophysical instead of photochemical deactivation pathways dominate their excited state dynamics.

Please do not adjust margins

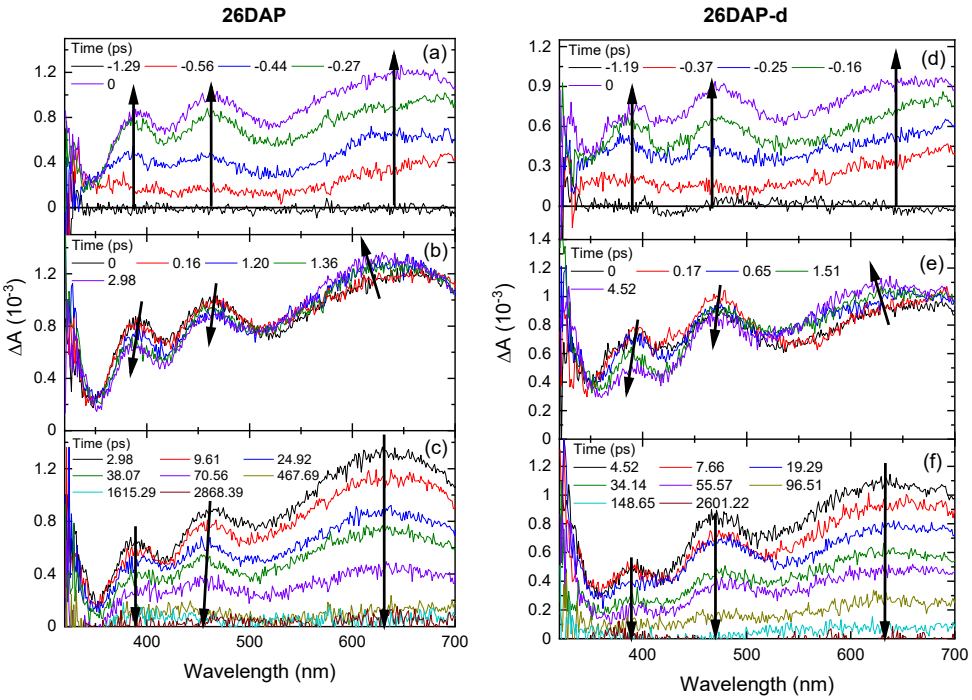

Figure 4. Transient absorption spectra of 26DAP (a-c) and 26DAP-d (d-f) in phosphate buffer pH 7.4, following 287 nm excitation. Time zero was determined at the maximum amplitude of absorption (Figure 4a and d) within the cross correlation of the pump and probe beams. Black arrows show the evolution of the transient absorption spectra in each panel.

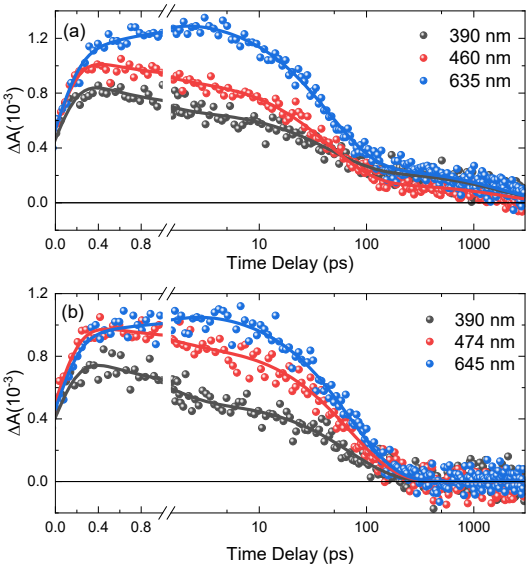

Figure 5. Representative decay traces of (a) 26DAP and (b) 26DAP-d in phosphate buffer pH 7.4 upon excitation with 287 nm. The solid lines show the best fit obtained from the global and target analyses.

Table 2. Lifetimes obtained from global and target analyses of the transient absorption data for 26DAP and 26DAP-d in phosphate buffer pH 7.4 upon excitation with 287 nm.

	τ_1 (ps)	τ_2 (ps)	τ_3 (ns)
26DAP	0.7 ± 0.1	43 ± 3	1.8 ± 0.6
26DAP-d	1.1 ± 0.1	70 ± 9	-

Discussion

Assignment of the transient absorption bands of 26DAP and 26DAP-d

The spectral dip observed in the transient absorption spectra of 26DAP and 26DAP-d at 345 nm (Figure 4) is assigned to stimulated emission, as these bands resemble the emission spectra reported for both molecules in Figure 2. Therefore, the transient absorption bands at ca. 640, 465, and 390 nm correspond to the excited state absorption spectrum of the $^1\pi\pi^*$ state, in agreement with the calculated excited state absorption spectra for the $^1\pi\pi^*$ minima of both tautomers in the C2-reaction coordinate (see Figure S9). In both molecules, after time-zero, the lowest-energy transient absorption band at ca. 640 nm blueshifts and increases its intensity, while the two higher-energy transient absorption bands at ca. 465 and 390 nm blueshift and decrease their intensity. We assign these dynamics to vibrational and conformational relaxation, and thus, the initial absorption of the $^1\pi\pi^*$ state observed in Figure 4a and d correspond to the vibrationally excited $^1\pi\pi^*$ state, while the transient absorption bands after the vibrational relaxation dynamics correspond to the absorption of the $^1\pi\pi^*$ state minimum of each molecule.

This journal is © The Royal Society of Chemistry 20xx

Please do not adjust margins

Proposed deactivation mechanism of 26DAP and 26DAP-d

Based on our experimental and theoretical results, we determined that 26DAP exists as a mixture of the N9 and N7 tautomers in phosphate buffer solution at pH 7.4, and thus, both tautomers must be considered to accurately describe the excited state dynamics of 26DAP. Following excitation with 287 nm, both tautomers will be excited to their corresponding $^1\pi\pi^*$ state. From the steady-state emission measurements for 26DAP and 26DAP-d, we can infer that the N7 tautomer has a higher fluorescence quantum yield than the N9 tautomer. We propose that the reason for the difference in the fluorescence yield among both tautomers is due to more excited state population remaining trapped in the $^1\pi\pi^*$ state minimum for the N7 tautomer than for the N9 because of the higher energy barrier (i.e., 0.8 vs. 0.4 eV) that must be overcome to access the CI_{C2}.

We are now in a position to propose a deactivation mechanism for 26DAP (Scheme 2). Upon 287 nm excitation, the $^1\pi\pi^*$ state of each tautomer is populated in the Franck-Condon region, and ultrafast branching of the population occurs following two coordinates: the C6-puckering and C2-puckering coordinates. This branching of the population in the Franck-Condon region is analogous to previous investigations in other purine derivatives.[44-46] The population following the C6-coordinate internally converts to the ground state through the CI_{C6} in an ultrafast time scale. The C2-coordinate involves a fraction of the population that internally converts to the ground state through the CI_{C2}, while a fraction of the population gets trapped in the $^1\pi\pi^*$ state minimum and decays radiatively to the ground state. As discussed above, the fraction that remains trapped in the $^1\pi\pi^*$ state minimum is higher in the N7 tautomer than in the N9 tautomer.

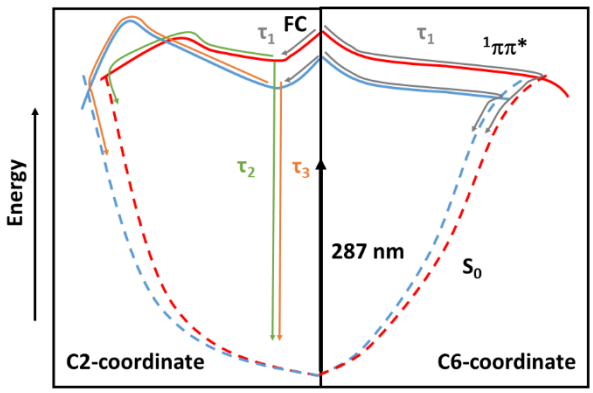

Scheme 2. Proposed electronic relaxation mechanism according to the experimental and theoretical results reported in this study. Note that the calculated vertical excitation energies vary between the N9 and N7 tautomers of 26DAP, and 26DAP-d, which is represented by the black arrow (Table 1). The red (N9 tautomer) and blue (N7 tautomer) solid lines represent the potential energy surface of the $^1\pi\pi^*$ state, while the dashed lines represent the potential energy surface of the ground state. τ_1, τ_2, and τ_3 are shown in colors gray, green, and orange, respectively.

We propose that τ_1 (0.7 ± 0.1 ps) corresponds to the branching of the excited-state population to either internally convert to the ground state through CI_{C6} or to populate the $^1\pi\pi^*$ state minimum following vibrational relaxation in the C2-coordinate. Considering the energy barrier that must be overcome to reach the CI_{C2}, τ_2 (43 ± 3 ps) is assigned to the simultaneous nonradiative internal conversion via CI_{C2} and fluorescence emission from the $^1\pi\pi^*$ minimum in the N9 tautomer, whereas τ_3 (1.8 ± 0.6 ns) is assigned to the same process in the N7 tautomer. Again, the lifetime for fluorescence emission of the N7 tautomer is longer than that of the N9 tautomer due to the higher energy barrier that must be overcome to access the CI_{C2} to decay nonradiatively to the ground state. We highlight that the 1.8 ± 0.6 ns lifetime is in good agreement with the fluorescence lifetime reported for 26DAP in water of 1.73 ± 0.01 ns.[34] The same deactivation mechanism applies for 26DAP-d, except that only one tautomer contributes to the observed dynamics. Therefore, τ_1 (1.1 ± 0.1 ps) corresponds to the branching of the excited-state population to either internally convert to the ground state through CI_{C6} or to populate the $^1\pi\pi^*$ state minimum following vibrational relaxation in the C2-coordinate. Similarly, τ_2 (70 ± 9 ps) is assigned to simultaneous internal conversion to the ground state via the CI_{C2} and fluorescence emission from the $^1\pi\pi^*$ minimum. As reported above, no evidence of long-lived excited states such as $^1n\pi^*$ or triplet states was detected in the transient absorption spectra shown in Figure 4. This evidences that photophysical (nonradiative internal conversion to the ground state and fluorescence emission) and not photochemical deactivation events dominate the excited state dynamics of 26DAP and 26DAP-d. Therefore, both molecules are expected to be reasonably photostable. This is further supported by the observation that 26DAP and 26DAP-d in phosphate buffer pH 7.4 only degraded by 2% and 8%, respectively, upon 287 nm excitation. These findings strengthen the likelihood that these purine derivatives could have participated in the formation of the proto-RNA or DNA oligomers and act as key components in the protection of the prebiotic genetic alphabet, enhancing the photostability of higher-order RNA or DNA structures.[13]

Conclusion

In this study, steady-state and time-resolved spectroscopies were complemented with electronic-structure calculations to provide a detailed description of the electronic relaxation mechanism of 26DAP and 26DAP-d. Importantly, the semi-quantitative calculations reported in this study can satisfactorily explain the experimental results. Scheme 2 summarizes the electronic relaxation mechanism. We proposed that upon excitation with 287 nm, the $^1\pi\pi^*$ state is populated, and in an ultrafast fashion, the population branches following the C2- and C6-coordinates as observed in other purine derivatives.[44-46] Following this branching event, the population that follows the C6-coordinate internally converts to the ground state through the CI_{C6} in an ultrafast time scale, while the population that follows the C2-coordinate vibrationally and conformationally relaxes to a $^1\pi\pi^*$ state minimum within τ_1. τ_2 and τ_3 correspond to the relatively slow nonradiative

This journal is © The Royal Society of Chemistry 20xx

Please do not adjust margins

Please do not adjust margins

internal conversion through the CI_{C2} and fluorescence emission from the $^1\pi\pi^*$ minimum of each N9 and N7 tautomers, respectively. A similar electronic relaxation mechanism is proposed for 26DAP-d, except that only one tautomer contributes to the observed dynamics. Based on our experimental and computational results, 26DAP and 26DAP-d may be considered photostable enough to have accumulated in significant quantities during the prebiotic era. Therefore, our results support the idea that 26DAP and 26DAP-d may have participated in the formation of prebiotic oligomers, acting as key components in the protection of the prebiotic genetic alphabet, and hence, possibly enhancing the photostability of higher-order RNA or DNA structures.[13]

Author contributions

Naishka E. Caldero-Rodríguez: investigation, formal analysis, writing-original draft, writing-review and editing
Luis A. Ortiz-Rodríguez: investigation, formal analysis, writing-original draft, writing-review and editing
Andres A. Gonzalez: investigation
Carlos E. Crespo-Hernández: conceptualization, funding acquisition, project administration, resources, supervision, visualization, validation, writing-review and editing

Conflicts of interest

There are no conflicts to declare.

Acknowledgments

The authors acknowledge funding from the National Science Foundation (Grant No. CHE-1800052). L.A.O-.R. also acknowledges the NSF-AGEP and the NOA-AGEP programs for support. This work made use of the High-Performance Computing Resource in the Core Facility for Advanced Research Computing at Case Western Reserve University.

References

1 J. Cadet, S. Mouret, J. L. Ravanat and T. Douki, *Photochem. Photobiol.*, 2012, **88**, 1048–1065.

2 W. J. Schreier, P. Gilch and W. Zinth, *Annu. Rev. Phys. Chem.*, 2015, **66**, 497–519.

3 J. Hidema, T. Kumagai, J. C. Sutherland and B. M. Sutherland, *Plant Physiol.*, 1997, **113**, 39–44.

4 A. A. Vink and L. Roza, *J. Photochem. Photobiol. B Biol.*, 2001, **65**, 101–104.

5 J.S. Taylor, *Acc. Chem. Res.*, 1994, **27**, 76–82.

6 V. Pages and R. P. P. Fuchs, *Oncogene*, 2002, **21**, 8957–8966.

7 A. Mees, T. Klar, P. Gnau, U. Hennecke, A. P. M. Eker, T. Carell and L.-O. Essen, *Science*, 2004, **306**, 1789–1793.

8 C. Tan, Z. Liu, J. Li, X. Guo, L. Wang, A. Sancar and D. Zhong, *Nat. Commun.*, 2015, **6**, 1–6.

9 W. L. de Laat, N. G. J. Jaspers and J. H. J. Hoeijmakers, *Genes & Dev.*, 1999, **13**, 768–785.

10 J. O. Fuss and P. K. Cooper, *PLoS Biol.*, 2006, **4**, e203.

11 Q. Mei and V. Dvornyk, *PLoS One*, 2015, **10**, e0135940.

12 W. Gehring and M. Rosbash, *J. Mol. Evol.*, 2003, **57**, S286--S289.

13 R. Szabla, M. Zdrowowicz, P. Spisz, N. J. Green, P. Stadlbauer, H. Kruse, J. Šponer and J. Rak, *Nat. Commun.*, 2021, **12**, 1–11.

14 M. P. Callahan, K. E. Smith, H. J. Cleaves, J. Ruzicka, J. C. Stern, D. P. Glavin, C. H. House and J. P. Dworkin, *Proc. Nat. Acad. Sci. U. S. A.*, 2011, **108**, 13995–13998.

15 M. D. Kirnos, I. Y. Khudyakov, N. I. Alexandrushkina and B. F. Vanyushin, *Nature*, 1977, **270**, 369–370.

16 I. Y. Khudyakov, M. D. Kirnos, N. I. Alexandrushkina and B. F. Vanyushin, *Virology*, 1978, **88**, 8–18.

17 Y. Zhou, X. Xu, Y. Wei, Y. Cheng, Y. Guo, I. Khudyakov, F. Liu, P. He, Z. Song, Z. Li, E. L. Ang, H. Zhao, Y. Zhang and S. Zhao, *Science*, 2021, **372**, 512–516.

18 C. Hartel and M. W. Göbel, *Helv. Chim. Acta*, 2000, **83**, 2541–2549.

19 E. I. Jiménez, C. Gibard and R. Krishnamurthy, *Angew. Chemie*, 2021, **133**, 10870–10878.

20 C. Sagan, *J. Theor. Biol.*, 1973, **39**, 195–200.

21 M. M. Brister, M. Pollum and C. E. Crespo-Hernández, *Phys. Chem. Chem. Phys.*, 2016, **18**, 22731.

22 J. R. Lakowicz, *Principles of Fluorescence Spectroscopy*, 2006.

23 F. Neese, F. Wennmohs, U. Becker and C. Riplinger, *J. Chem. Phys.*, 2020, **152**, 224108.

24 A. D. Becke, *J. Chem. Phys.*, 1993, **98**, 5648–5652.

25 T. H. Dunning Jr, *J. Chem. Phys.*, 1989, **90**, 1007–1023.

26 V. Barone and M. Cossi, *J. Phys. Chem. A*, 1998, **102**, 1995–2001.

27 F. Neese, F. Wennmohs, A. Hansen and U. Becker, *Chem. Phys.*, 2009, **356**, 98–109.

28 A. D. Becke, *Phys. Rev. A*, 1988, **38**, 3098.

29 F. Weigend and R. Ahlrichs, *Phys. Chem. Chem. Phys.*, 2005, **7**, 3297–3305.

30 C. Reichardt, R. A. Vogt and C. E. Crespo-Hernández, *J. Chem. Phys.*, 2009, **131**, 224518.

31 J. J. Snellenburg, S. P. Laptenok, R. Seger, K. M. Mullen, I. H. M. van Stokkum, *J. Stat. Softw.*, 2012, **49**, 1–22.

32 A. Albert and B. J. Brown, *J. Chem. Soc.*, 1954, 2060–2071.

33 D. C. Ward, E. Reich and L. Stryer, *J. Biol. Chem.*, 1969, **244**, 1228–1237.

34 P. Virta, A. Koch, M. U. Roslund, P. Mattjus, E. Kleinpeter, L. Kronberg, R. Sjöholm and K. D. Klika, *Org. & Biomol. Chem.*, 2005, **3**, 2924–2929.

35 H. DeVoe and S. P. Wasik, *J. Solution Chem.*, 1984, **13**, 51–60.

 This journal is © The Royal Society of Chemistry 20xx

Please do not adjust margins

Please do not adjust margins

36 C. Santhosh and P. C. Mishra, *Spectrochim. Acta A*, 1991, **47**, 1685–1693.

37 B. Cohen, P. M. Hare and B. Kohler, *J. Am. Chem. Soc.*, 2003, **125**, 13594–13601.

38 C. Reichardt, C. W. Wen, R. A. Vogt and C. E. Crespo-Hernández, *Photochem. Photobiol. Sci.*, 2013, **12**, 1341–1350.

39 C. E. Crespo-Hernández, L. Martínez-Fernández, C. Rauer, C. Reichardt, S. Mai, M. Pollum, P. Marquetand, L. González and I. Corral, *J. Am. Chem. Soc.*, 2015, **137**, 4368–4381.

40 E. Mburu and S. Matsika, *J. Phys. Chem. A*, 2008, **112**, 12485–12491.

41 M. A. El-Sayed, *J. Chem. Phys.*, 1962, **36**, 573–574.

42 M. A. El-Sayed, *J. Chem. Phys.*, 1963, **38**, 2834–2838.

43 B. G. Levine, C. Ko, J. Quenneville and T. J. Martínez, *Mol. Phys.*, 2006, **104**, 1039–1051.

44 B. Ashwood, L. A. Ortiz-Rodríguez and C. E. Crespo-Hernández, *Faraday Discuss.*, 2018, **207**, 351–374.

45 B. Ashwood, L. A. Ortiz-Rodríguez and C. E. Crespo-Hernández, *J. Phys. Chem. Lett.*, 2017, 4380–4385.

46 P. Zhou and L. Zhao, *J. Phys. Chem. B*, 2018, **123**, 201–206.

This journal is © The Royal Society of Chemistry 20xx

Please do not adjust margins